Steel and Composite Structures, *Vol. 17, No. 6 (2014) 951-965*
DOI: http://dx.doi.org/10.12989/scs.2014.17.6.951

Inelastic response of wide flange steel beams curved by symmetrical weak axis bending using two-point loads

Antoine N. Gergess [*1] and Rajan Sen [2]

[1] *Department of Civil Engineering, University of Balamand, Al-Koura, P.O. Box 100, Lebanon*
[2] *University of South Florida, Tampa, Florida, USA*

(*Received May 11, 2012, Revised November 12, 2013, Accepted April 30, 2014*)

Abstract. Point bending is commonly used for cambering and curving steel girders to large radii. In this system, a hydraulic ram or press is used to apply concentrated loads at selected points to obtain the required vertical (cambering) or horizontal (curving) curved profile from induced permanent deformations. This paper derives closed form solutions that relate loads to permanent deformations for horizontally curving wide flange steel beams based on their post-yield response. These solutions are presented in a parametric form to identify the relationship between key variables and their impact on the accuracy of the curving operation. It is shown that point bending could yield parabolic curved profiles that are within 1% of a desired circular curve if the span length to radius of curvature ratio (L/R) is less than 1.5 and the point loads are spaced at one third the beam length. Safe limits are then established on loads, strains and curvatures to avoid damaging the steel section. This leads to optimization of the point bending operation for inducing a circular profile in wide flange steel beams of any size.

Keywords: steel; wide flange; non-linear; point bending; radius; inelastic

1. Introduction

Point bending is used in building construction for cambering and curving steel girders. In cambering, the girder is bent about its strong axis to induce a vertical curve (Fig. 1(a)) to compensate for dead / live load deflection. In curving, the steel girder is bent about its weak axis (Fig. 1(b)) to induce a horizontal curve to match a specific geometric and/or architectural profile. This profile is typically circular.

The desired profile is obtained by a single application of mechanical loads at selected points, usually at the third points (Bjorhovde 2006). Point bending systems are ideal for large radii (Alwood 2006) because the parabolic deformed shape induced by applied loading closely matches the required circular profile.

Recently, the authors formalized the point bending procedure for cambering wide flange steel girders by deriving closed-form solutions that relate applied loads to permanent deformations and curvatures (Gergess and Sen 2010) based on the plastification of steel (Moen and Via 2011), Fig. 2.

∗Corresponding author, Ph.D., PE, F.ASCE, Full Professor, E-mail: tgeorges@balamand.edu.lb
[a] Ph.D., PE, F.ASCE, ACI, Professor and Jefferson Science Fellow, E-mail: sen@usf.edu

http://www.techno-press.org/?journal=scs&subpage=8 ISSN: 1229-9367 (Print), 1598-6233 (Online)

This paper extends this solution to applications for inducing a horizontal profile, that is, weak axis bending.

(a) Strong axis bending (Cambering)

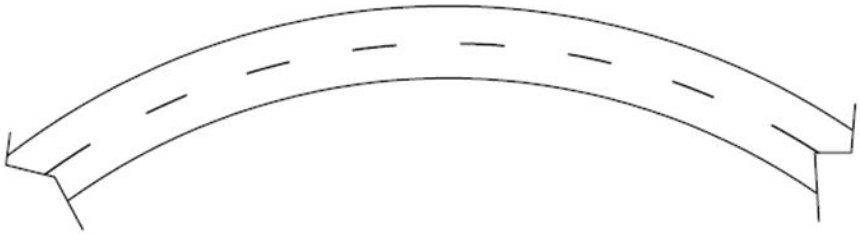

(b) Weak axis bending (Curving)

Fig. 1 Curving wide flange steel girders (King 2005)

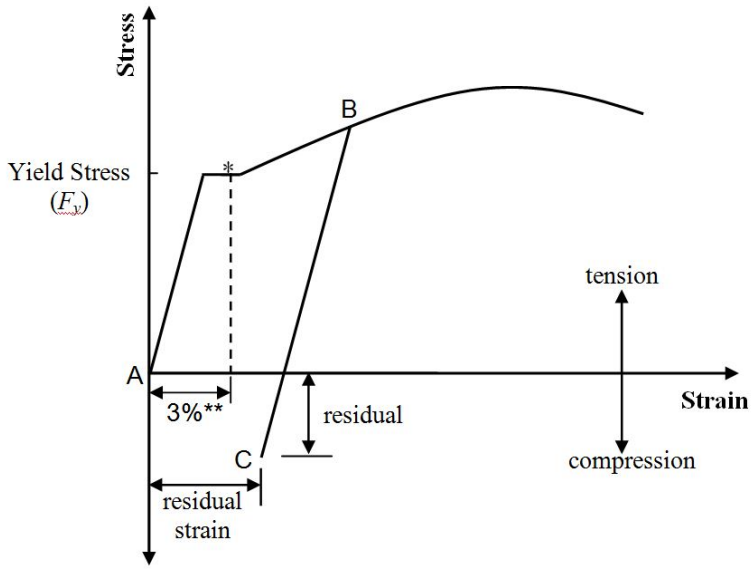

* yield plateau: length varies from 10 to 20 times the yield strain ε_y
** typical value used by fabricators before steel properties are reduced (Lange 2009)

Fig. 2 Idealized stress-strain curve for Grade 250 and 345 steel (Moen and Via 2011)

2. Approach

Closed-form solutions relating point loads to residual deformations were previously derived (Gergess and Sen 2011). These solutions are re-cast in a parametric form to limit the number of variables and simplify the solution. The intent is to provide practical solutions that can be readily used to predict the magnitude of the required load and ensure that the corresponding deformations and strains fall within permissible code limits (AISC 2011). Residual deformations are then plotted to determine the sensitivity of the solution to variations in the magnitude of the parameters.

To make the solution useable, the non-linear solution focuses on available AISC rolled wide flange sections (W1100 × 499 to W100 × 19.3, Fig. 3) (AISC 2011) corresponding to Grade 250 and Grade 345 steel, as well as Grade 415 steel that is representative of the measured yield stress value for Grade 345 steel (Brockenbrough 2003). Maximum strains are limited to 3% (Fig. 2), a typical value used by fabricators before steel properties are reduced (Lange and Grages 2009). This allows the analysis to be conducted based on elastic-perfectly plastic stress-strain behavior and ensures that the yield stress in tension and compression remain the same (e.g., Bauschinger effects do not have to be considered).

3. Description of the point bending system

Point bending uses mechanical loads to develop the required curved profile. Point bending machines consist of a steel frame in which the hydraulic jacks are horizontally mounted on one side of the flanges with a reaction beam supported on two points placed on the opposite side of the flanges (Bjorhovde 2006) (Fig. 4(a)).

3.1 Girder geometry

The design length of the fabricated straight girder is defined as L. The actual length of the

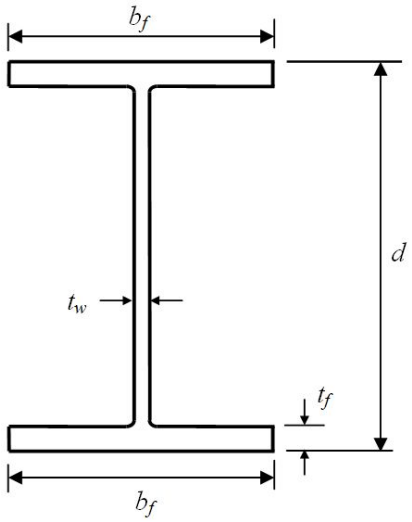

Fig. 3 Cross-section of a rolled *W* shape (AISC 2011)

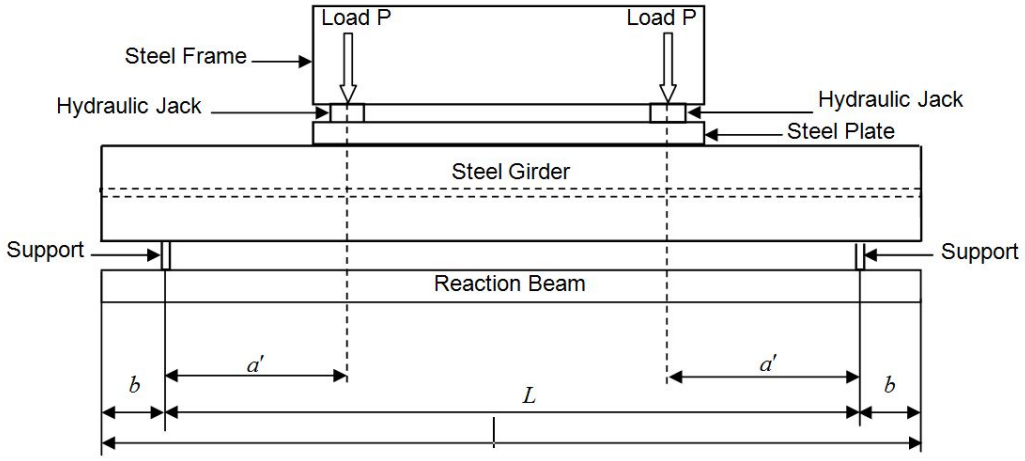

* Length $L' = L + 2b$

(a) Point bending steel rolled shapes (weak axis bending)

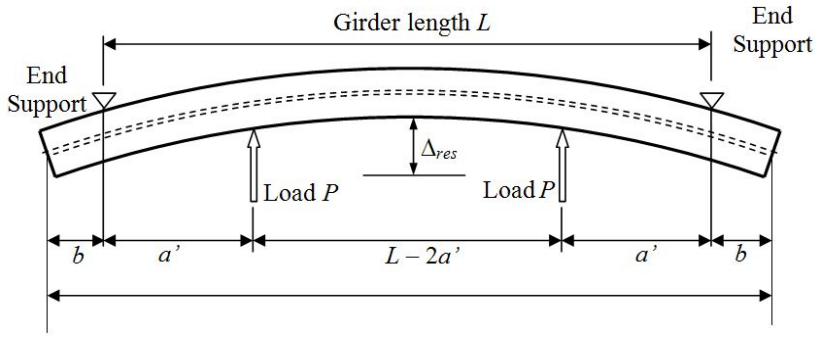

* Actual length $L' = L + 2b$

(b) Development of curved shape based on point bending

* Actual girder length is $L' = L + 2b$ ($b \approx 0.05L$ e.g., $L' \approx 1.1L$). Dimension b to be trimmed after completing the cold curving operation (Alwood 2006)

Fig. 4 Idealization of the point bending operation

girder, L', is longer to satisfy placement requirements within the bending machine (Alwood 2006). Thus, $L' = L + 2b$, where the dimension b is the distance from the end supports of the reaction beam to the end of the girder (Fig. 4(a)). The distance b is usually set at $0.05L$ so that $L' \approx 1.1L$. The overhang length is trimmed after the point bending operation is completed (Alwood 2006).

3.2 Load application

The point bending set-up for weak axis bending is shown schematically in Fig. 4(a) where two equal concentrated loads P, distant a' from the supports, are applied incrementally until the desired curved profile is attained (Fig. 4(b)).

3.3 Idealization of curved shape

Point loads (Fig. 4(a)) are typically applied at the third point ($a' = L/3$, Fig. 4(a)) to ensure a smooth parabolic shape (Fig. 4(b)) (Bjorhovde 2006). In cambering, this profile almost exactly compensates for dead and live load deflections; however, it is less than ideal where the required curve is an arc of a circle as shown in Fig. 5.

For a girder length L and desired radius of curvature R, the mid-span ordinate (which corresponds to the maximum induced deformation) is the key variable. From geometry, $\delta_{max} = R\left(1-\sqrt{1-\left(\frac{L}{2R}\right)^2}\right)$ (AISC 2011). At a distance x from the girder end, the ordinates can be calculated using the equations given in Fig. 5 for both circular and parabolic shapes. The mismatch between the circular and parabolic curves is most noticeable for small radii mainly for span length to radius of curvature ratio (L / R) larger than 1.5 (as shown in Section 6.1 in the paper). Consequently, the applicability of the point bending technique is recommended for $L/R \leq 1.5$. Note that there are alternative bending techniques such as three-roller bending and heat curving that may be used for smaller radii (Bjorhovde 2006).

4. Analytical solution

The maximum deflection (δ_{max} in Fig. 5) corresponds to the residual displacement following application and release of the point loads (Fig. 4(b)). For cambering (Gergess 2010), AISC sets limits on the minimum camber radius R as a function of the girder depth to avoid excessive straining of the extreme fibers of the section. These limits do not apply for curving because the required bending loads are smaller (due to weak axis bending compared to strong axis bending in cambering). However, the lateral stability requirements in curving are quite different. Unlike cambering where the web is considered to be stiffened by the top and bottom flanges, in curving the flange is considered to be un-stiffened because there are no flexural stresses at the flange/web junction, Fig. 6 (Bjorhovde 2006).

Local flange buckling can be avoided by controlling the magnitude and spacing of the applied loads. The recommended spacing between the point loads is based on the lateral bracing limit L_p set by AISC. For girders where the flexural capacity is governed by plastic bending (Wong and Driver 2010), it is given by Eq. (1) as (AISC 2011)

$$L_p = 0.255 b_f \sqrt{\frac{E}{F_y}} \tag{1}$$

where b_f is the flange width, E is the modulus of elasticity and F_y is the yield stress.

The magnitude of the load applied to each flange ($P_{flange} = P/2$) is limited to the allowable strength for the limit state of flange local buckling (AISC 2011) and is given by Eq. (2) as

$$P_{flange} \leq 3.75 t_f{}^2 F_y \Rightarrow P \leq 7.5 t_f{}^2 F_y \tag{2}$$

where F_y is in MPa, t_f (flange thickness) in mm and P_{flange} (load per flange) in N.

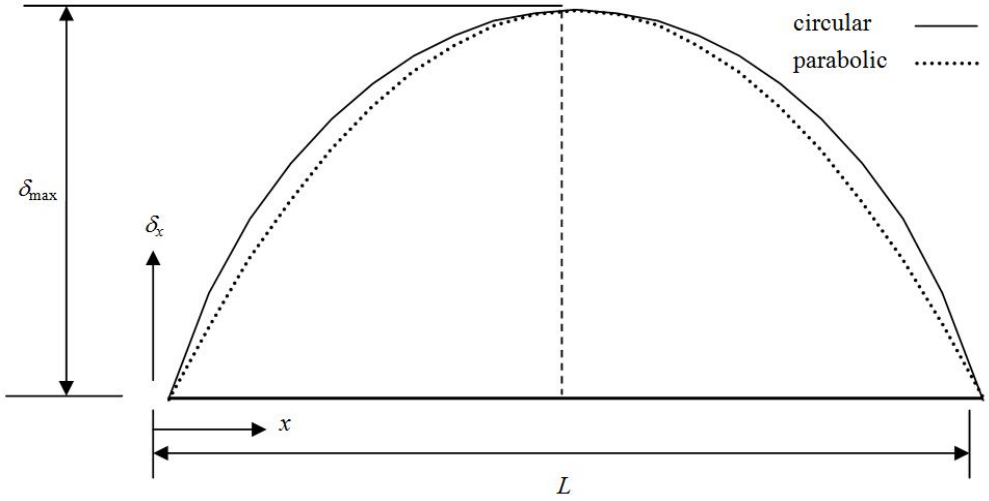

$$\delta_{\max} = R - \sqrt{R^2 - \frac{L^2}{4}}$$

$$\text{circular}: \ \delta_x = \sqrt{R^2 - \left(x - \frac{L}{2}\right)^2} - \sqrt{R^2 - \frac{L^2}{4}}$$

$$\text{parabolic}: \ \delta_x = -\frac{4\delta_{\max}}{L^2}x^2 + \frac{4\delta_{\max}}{L}x$$

Fig. 5 Idealized curved shape (Bjorhovde 2006)

In case the flange buckling criteria (Eqs. (1) and (2)) are not satisfied, temporary transverse stiffeners can be provided at intermediate points along the girder length and removed later.

4.1 Induced deformations

The applied post-yield loads induce permanent deformations in the girder. Expressions for the inelastic load P, the induced inelastic Δ_p, elastic Δ_e and residual deformations Δ_{res} were previously derived (Gergess and Sen 2011). In these expressions, the key variables are the girder flange dimensions (flange width b_f and thickness t_f, Fig. 3), the girder length L (that is also the distance between the reaction arms of the bending frame, Fig. 4), the offset of the load points a' (Fig. 4), the point at which yield is initiated x_2 (Fig. 6), the steel grade F_y and the modulus of elasticity E (Fig. 2). It should be noted that the restraining effect of the web on the post-yield loads and deformations of the steel girder is neglected since its stiffness in weak axis bending is small in comparison to that of the flanges.

To reduce the number of variables, these equations are re-cast in a parametric form and the relationships between key variables established.

4.2 Parameters

Two parameters τ and χ are defined. Parameter τ is the ratio of the offset of the load points a' to the bending span L ($\tau = a' / L$), usually set at one third the span length for inducing circular curves (Bjorhovde 2006). Parameter χ is the ratio of the distance where yield initiates (x_2) to the offset of the load points a' ($\chi = x_2 / a'$), Fig. 6.

4.3 Inelastic loads

The expression for the post-yield load P for the two flanges (based on elasto-plastic analysis) (Gergess 2011) re-cast using parameters τ and χ is given by Eq. (3) as

$$P = \frac{F_y t_f b_f^{\,2}}{3\tau\chi L} \Rightarrow P = \frac{F_y t_f b_f^{\,2}}{\chi L} \quad (\text{for } \tau = 1/3) \tag{3}$$

4.4 Residual deformation Δ_{res}

The closed form equation for the residual deformation Δ_{res} that develops after release of the post-yield load is obtained by subtracting the elastic deformation Δ_e due to unloading from the inelastic deformation Δ_p (Craig 2011).

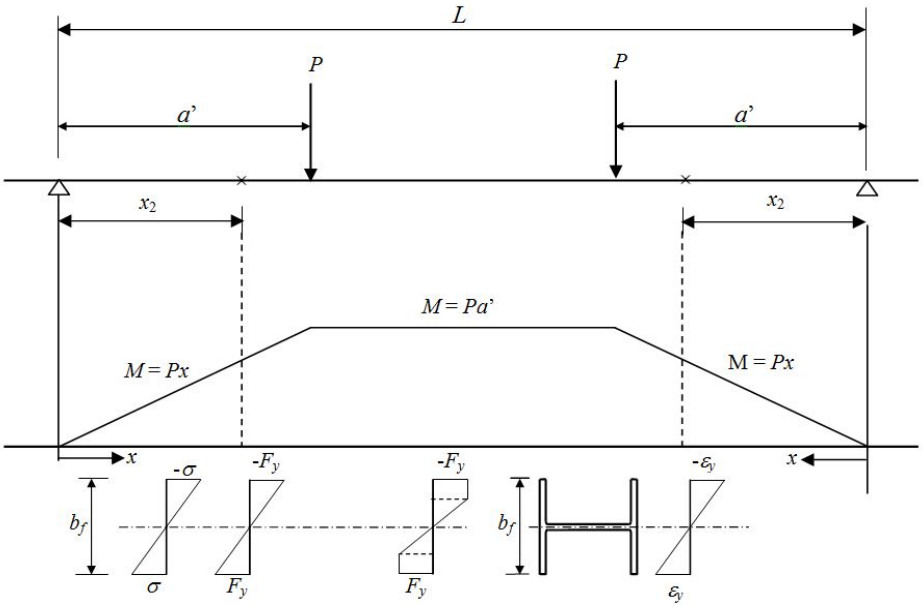

Stress diagram:	elastic	yield	inelastic
	$0 < x \le x_2$	$x = x_2$	$x_2 < x < L/2$

* Note: $x_2 = 2L/3$ when the section becomes fully plastic at mid-span

Fig. 6 Stress variation with the bending span L

The residual deformation Δ_{res} normalized with respect to the girder length squared to flange width ratio (L^2/b_f) is presented in a parametric form in Eq. (4) so it can be plotted as a function of parameters χ and τ

$$\left(\frac{\Delta_{res}}{\frac{L^2}{b_f}}\right)=\frac{F_y}{E}\left(\left[\frac{1}{\sqrt{3-\frac{2}{\chi}}}\left(\frac{1}{4}-\tau^2\right)-2(\chi\tau)^2\left(1+\frac{1}{3\chi}\right)\sqrt{3-\frac{2}{\chi}}+\frac{10}{3}(\chi\tau)^2\right]-\left[\frac{1}{3\chi}\left(\frac{3}{4}-\tau^2\right)\right]\right) \tag{4}$$

Inelastic Δ_p Elastic Δ_e

Setting τ as 0.33, Eq. (4) is re-written in Eq. (5) for $\tau = 1/3$ as follows

$$\left(\frac{\Delta_{res}}{\frac{L^2}{b_f}}\right)=\frac{F_y}{E}\left(\left[\frac{5}{36}\frac{1}{\sqrt{3-\frac{2}{\chi}}}-\frac{2}{9}\chi^2\sqrt{3-\frac{2}{\chi}}-\frac{2}{27}\chi\sqrt{3-\frac{2}{\chi}}+\frac{10}{27}\chi^2\right]-\left[\frac{23}{108\chi}\right]\right) \tag{5}$$

Inelastic Δ_p Elastic Δ_e

Note that in Eqs. (4) and (5) both the inelastic deformation Δ_p that develops during loading and the elastic deformation Δ_e that develops during unloading are labelled.

5. Parametric analysis

The mathematical derivations show that χ and τ are the only parameters that vary in the closed form expressions for induced deformations (Eqs. (4)-(5)). The parameter τ is one third the girder length L and χ varies from 2/3 to 1 (so that the term under the square root in Eqs. (4) and (5) is real).

The variation of $\Delta_{res}/(L^2/b_f)$ in Eq. (5) with χ is plotted in Fig. 7. The ordinate of the plot $\Delta_{res}/(L^2/b_f)$ is multiplied by 10,000 for clarity. The variation in χ is shown in increments of 0.005 starting at χ = 0.667 and ending at χ = 0.695 to highlight its contribution to the point bending operation (values for χ larger than 0.695 are not shown as they are insignificant).

Fig. 7 contains three plots, corresponding to the three different steel grades (Grades 250, 345 and 415) considered in this paper. It may be seen that at χ = 0.667, $\Delta_{res}/(L^2/b_f) \times 10{,}000$ is 42 for Grade 250, 59 for Grade 345 and 71 for Grade 415 steel. These values reduce significantly at χ = 0.695 to $\Delta_{res}/(L^2/b_f) \times 10{,}000 = 2.7$ for Grade 250, 3.7 for Grade 345 and 4.4 for Grade 415 steel, that is, a 4% increase in χ (from 0.667 to 0.695) can reduce deformations Δ_{res} (e.g., radii of curvatures R) almost 16 fold. This quantifies the sensitivity of an increase in deformation to the onset of yield in the post-yield range.

Since the point load P is inversely proportional to χ (Eq. (3)), the curving radius can be reduced dramatically by minor increases in the bending load P in the post-yield regime. The analytical solution reflects ideal conditions that are not completely realizable in practice in part because actual material properties vary (Brockenbrough 2003). Nonetheless, it gives a good indication on the magnitude of the loads required for curving.

6. Range of curvatures, loads and strains

Based on the parametric analysis and the variation of $\Delta_{res} / (L^2 / b_f)$ with χ in Fig. 7, the ranges for curvatures, strains and loads are set as follows:

6.1 Curvature

As shown in Fig. 5, a circular shape is approximated by a parabola. The accuracy of this approximation depends on the radius of curvature, that is, the larger the radius, the better the approximation. By comparing deformations at intermediate points using the closed form expressions for circular and parabolic deformed shapes in Fig. 5, it was found that they are identical for $L/R \le 1$, 1% different for $L/R = 1.5$, 3% different for $L/R = 1.75$ and 15% different for $L/R = 2$. Consequently, this approach is considered to be reasonably accurate if the ratio of the girder length L to the radius of curvature R is limited to 1.5 ($L/R \le 1.5$).

The expression for Δ_{res} in Fig. 4(b) ($\delta_{\max}$ in Fig. 5) is recast as a function of the flange width to the radius of curvature ratio (b_f / R) so that the range of curvatures for standard AISC rolled W shapes (AISC 2011) can be determined. This is given by Eq. (6) which is a function of L/R and $\Delta_{res} / (L^2 / b_f)$

$$\frac{b_f}{R} = \frac{\left(\frac{L}{R}\right)^2 \left(\frac{\Delta_{res}}{\frac{L^2}{b_f}} \right)}{\left(1 - \sqrt{1 - 0.25\left(\frac{L}{R}\right)^2} \right)} \tag{6}$$

If L/R in Eq. (6) is set to its limiting value of 1.5 ($L/R \le 1.5$), the limit on the flange width to radius of curvature ratio (b_f / R) is given by Eq. (7)

$$\frac{b_f}{R} \ge 6.65 \left(\frac{\Delta_{res}}{\frac{L^2}{b_f}} \right) \tag{7}$$

Consequently, the limit on the radius is given by expressing R from Eq. (7) as a function of b_f in Eq. (8)

$$R \le 0.15 b_f / \Delta_{res} / (L^2 / b_f) \tag{8}$$

This makes R a function of the normalized residual deformation $\Delta_{res} / (L^2 / b_f)$ and the flange width b_f. For rolled W shapes (AISC 2011), the flange width b_f varies from 100 mm (W150 × 13) to 457 mm (W920 × 1191). Fig. 7 shows that $\Delta_{res} / (L^2 / b_f) \times 10^4$ varies from 2.7 to 42 for Grade 250, 3.7 to 59 for Grade 345 and 4.4 to 71 for Grade 415 steel.

Based on the upper-bound values of $\Delta_{res} / (L^2 / b_f)$ (that is, 42, 59 and 71 multiplied by 10^{-4}),

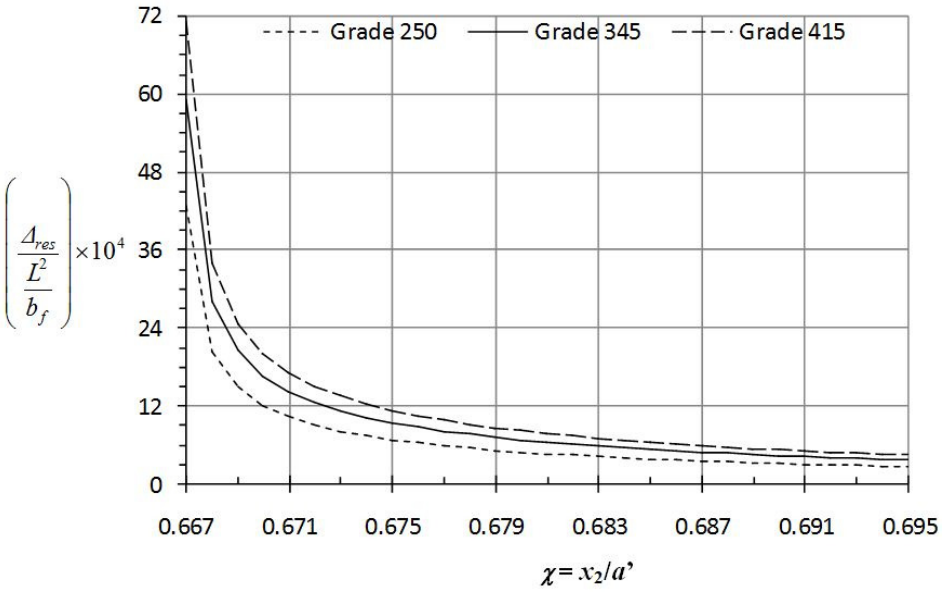

Fig. 7 Plots for Residual deformations ($\tau = 1/3$)

limits on the radii of curvature are set as: $R \geq 16.5$ m (Grade 250), $R \geq 12$ m (Grade 345) and $R \geq 10$ m (Grade 415) steel for $b_f = 457$ mm and $R \geq 4$ m (Grade 250), $R \geq 3$ m (Grade 345) and $R \geq 2.5$ m (Grade 415) steel for $b_f = 100$ mm. Table 1 summarizes the range of curvatures that can be induced for the upper-bound and lower-bound values of $\Delta_{res} / (L^2 / b_f)$ using point bending for curving the girder about its weak axis.

6.2 Strain

The residual strain is calculated from its usual relationship with curvature $1/R \Rightarrow \varepsilon / y = 1/R$ where y is taken at the flange tip ($y = b_f / 2$) (Fig. 3). Substituting ε by $b_f / 2R$ in Eq. (7) results in the following expression for the maximum residual strain

$$\varepsilon = \frac{b_f}{2R} = 3.325\left(\frac{\Delta_{res}}{\frac{L^2}{b_f}}\right) \tag{9}$$

Based on the upper-bound values of $\Delta_{res} / (L^2 / b_f)$ (that is, 42, 59 and 71 multiplied by 10^{-4}), limits on residual strains are set as: $\varepsilon = 3.325 \times 42 \times 10^{-4} = 0.014$ for Grade 250, $\varepsilon = 3.325 \times 59 \times 10^{-4} = 0.02$ for Grade 345 and $\varepsilon = 3.325 \times 71 \times 10^{-4} = 0.024$ for Grade 415 steel.

It is customary to express post-yield strains as multiples of the initial yield strain ε_y (Fig. 2). The yield strain values for the three grades of steel considered in this paper are 0.00125 for Grade 250, 0.00173 for Grade 345 and 0.00208 for Grade 415 steel. Using these values, the corresponding maximum strains ($\varepsilon = 0.014$ for Grade 250, $\varepsilon = 0.02$ for Grade 345 and $\varepsilon = 0.024$ for Grade 415

steel) work out to approximately $11.5\varepsilon_y$, the same value for all three steel grades. This is because the yield stress F_y is a common factor in the expression for $\Delta_{res} / (L^2 / b_f)$ in Eq. (5).

While the permanent residual strain (ε) develops *after* removal of the point loads, the actual strain that develops *during* loading is greater (labeled as $\varepsilon_{\max}$) because there is no elastic rebound. $\varepsilon_{\max}$ can be determined by an expression similar to Eq. (9) except that the residual deformation Δ_{res} is replaced by the inelastic deformation component (Δ_p) in Eq. (5). Δ_p is 1.1 times the residual displacement Δ_{res} (determined mathematically from Eq. (5) as the ratio of the inelastic deformation component Δ_p to the elastic deformation component Δ_e for $\chi = 0.667$). Thus, $\varepsilon_{\max} = 1.1\varepsilon = 1.1 \times 11.5\varepsilon_y = 12.65\varepsilon_y$ for Grade 250, 345 and 415 steel. This maximum strain falls within the yield plateau of conventional steel at 10 to $20\varepsilon_y$ (Salmon 2010) thus ensuring that steel is not strained into the strain hardening range e.g., the change in the mechanical properties of steel is not substantial (Barnshaw 2009). According to fabricators, steel sections can be curved up to approximately 3% strain without compromising their performance (Lange and Grages 2009). This limit corresponds to $24\varepsilon_y$ for Grade 250, $17.4\varepsilon_y$ for Grade 345 and $14.5\varepsilon_y$ for Grade 415 steel and is larger than the maximum value ($\varepsilon_{\max} = 12.65\varepsilon_y$) specified in this paper.

6.3 Range of point loads P

The maximum bending load P is dictated by flange buckling (AISC 2011) where the limiting flange buckling load ($P_{\text{flange}} = P/2$) is given by Eq. (2). For the range of AISC rolled W shapes, t_f varies from 4.95 mm for W150 × 13 to 125 mm for W360 × 1086. Substituting the two extreme values for t_f and the steel yield stress, a limiting load range can be calculated that is summarized in Table 1.

It may be seen from Table 1 that the limiting load P (per girder) varies from 46 kN (t_f = 4.95 mm for W150 × 13, Grade 250) up to 48500 kN (t_f = 125 mm for W360 × 1086, Grade 415). In practice, fabricators prefer to set a limit of 10000 kN (1000 metric tons), a typical value of hydraulic jacks' capacity.

Table 1 Range of radii of curvatures and point loads

Ranges	Grade 250	Grade 345	Grade 415
χ	$0.667 \le \chi \le 0.695$	$0.667 \le \chi \le 0.695$	$0.667 \le \chi \le 0.695$
$\Delta_{res} / (L^2 / b_f) \times 10^4$	$3 \le \Delta_{res} / (L^2 / b_f) \times 10^4 \le 42$	$4 \le \Delta_{res} / (L^2 / b_f) \times 10^4 \le 59$	$5 \le \Delta_{res} / (L^2 / b_f) \times 10^4 \le 71$
$b_f / R \times 10^4$	$20 \le (b_f / R \times 10^4) \le 279$	$27 \le (b_f / R \times 10^4) \le 392$	$33 \le (b_f / R \times 10^4) \le 472$
b_f (mm)	$100 \le b_f \le 457$	$100 \le b_f \le 457$	$100 \le b_f \le 457$
R (m)	$4 \le R \le 50$ for b_f = 100 mm $16.5 \le R \le 229$ for b_f = 457 mm	$3 \le R \le 41$ for b_f = 100 mm $12 \le R \le 186$ for b_f = 457 mm	$2.5 \le R \le 30$ for b_f = 100 mm $10 \le R \le 138$ for b_f = 457 mm
t_f (mm)	$4.95 \le t_f \le 125$	$4.95 \le t_f \le 125$	$4.95 \le t_f \le 125$
Limits on bending loads P (kN)	$46 \le P \le 29000$	$63 \le P \le 40000$	$76 \le P \le 48500$

7. Optimization of point bending set-ups

7.1 Set-ups

Point bending makes use of dual load (Fig. 4(a)) applications to induce curvatures. A girder of length L is placed horizontally in a steel frame (Fig. 4, selfweight is neglected) where loads are applied using hydraulic jacks until the desired curve is attained (Fig. 4(b)). The longitudinal arms of the frame spaced at L constitute the end supports (placed symmetrically at a distance b from the ends, Fig. 4(a)). Based on common practice, b is set at $0.05L$ ($L' = 1.1L$).

7.2 Point loads and induced residual deformations

The maximum residual deformation that develops at mid-span of the girder of length L is approximated as $\Delta_{res} = R\left(1-\sqrt{1-\left(\frac{L}{2R}\right)^2}\right)$ (Fig. 5) where R is the desired radius. From Fig. 7, the onset of yield (parameter χ) can be depicted as a function of the steel grade and the ratio Δ_{res} / (L^2 / b_f) × 10,000 (normalized residual deformation with respect to the girder length squared to flange width ratio). The point load per girder (P) is then determined from Eq. (3) as a function of the yield stress (F_y), flange thickness (t_f), flange width (b_f), girder length (L) and parameter χ ($P = F_y t_f b_f^2 / \chi L$).

7.3 Limits

Limits on point loads spacing and magnitude are based on AISC to prevent localized damage (Eq. (1): $\frac{L}{3} \le 0.255 b_f \sqrt{\frac{E}{F_y}}$ and Eq. (2): $P \le 7.5 t_f^2 F_y$) and avoid using stiffeners to control lateral buckling during bending (White 2008).

Limits on the desired radius of curvature (R) are set based on geometric idealization between parabolic and circular shapes (Eq. (7): $L/R \le 1.5$ and $b_f / R \ge 6.65 \times (\Delta_{res} / (L^2 / b_f))$. In case these conditions are not satisfied, the point bending operation can be accomplished in stages e.g., the point loads are reconfigured to induce half the curvature (that is twice the radius $2R$) in each stage. In this case, residual stresses that build-up during the first load stage are neglected as they may be released by heat treatment (Spoorenberg *et al*. 2010).

8. Application

The inelastic response of wide flange steel beams curved by point bending is illustrated by a numerical application. In the example, a 10 m long, Grade 345 W410 × 60 girder is to be curved to a radius of 15 m. It is required to determine the optimal point bending set-up. The sensitivity of induced deformations to variation in loads is also illustrated by reducing the radius to 7.5 m (by half) and 5 m (by two third).

8.1 Solution for R = 15 m

The girder cross-sectional properties are first obtained from the AISC Manual. These are the flange width b_f = 17.8 cm, the flange thickness t_f = 1.28 cm, the girder length L = 10 m (the actual girder length is set at L' = 1.1L = 11 m for fitting purposes), the steel yield stress F_y = 345 MPa and the radius of curvature R = 15 m.

Based on the given data, the maximum mid-span residual deformation corresponding to point loads applied at third-points (e.g., L/3 = 10 m / 3 = 3.33 m), is approximated as $\Delta_{res} = R\left(1-\sqrt{1-\left(\frac{L}{2R}\right)^2}\right) = 15\left(1-\sqrt{1-\left(\frac{10}{2\times 15}\right)^2}\right) = 0.858$ m (Fig. 5).

From Fig. 7, based on $\Delta_{res} / (L^2 / b_f) \times 10{,}000 = 0.858 / (10^2 / 0.178) \times 10{,}000 = 15.3$, parameter χ is scaled as 0.67 (Grade 345). From Eq. (3), the point load P is calculated as $P = F_y t_f b_f^2 / \chi L$ = 345 × 1000 × 0.0128 × (0.1782^2) / 0.67 × 10 = 20.9 kN which is smaller than the limiting value of $7.5 t_f^2 F_y$ equal to 7.5 × 12.8^2 × 345 / 1000 = 424 kN. Since the spacing between the loads (L / 3 = 3.33 m) is larger than the limiting value $L_p = 0.255 b_f \sqrt{\frac{E}{F_y}} = 0.255 \times 0.178 \sqrt{\frac{200000}{345}}$ = 1.1 m, removable transverse stiffeners should be attached along the girder length during bending.

The accuracy of the point bending operation is finally checked by ensuring that L/R = 10 / 15 = 0.67 < 1.5 and b_f/R = 0.178 / 15 = 0.012 > 6.65 × (Δ_{res} / (L^2 / b_f)) = 6.65 × 15.3 × 10^{-4} = 0.0102.

8.2 Solution for R = 7.5 m

If the radius of curvature R is reduced to 7.5 m, the residual deformation Δ_{res} increases to $7.5\left(1-\sqrt{1-\left(\frac{10}{2\times 7.5}\right)^2}\right)$ = 1.91 m. From Fig. 7, based on $\Delta_{res} / (L^2 / b_f) \times 10{,}000$ = 1.91 / (10^2 / 0.178) × 10,000 = 34, parameter χ is scaled as 0.668 (Grade 345). From Eq. (3), the point load P is calculated as $P = F_y t_f b_f^2 / \chi L$ = 345 × 1000 × 0.0128 × (0.1782^2) / 0.668 × 10 = 21 kN, almost equal to the 20.9 kN load used to induce the radius of 15 m. This highlights the sensitivity of the variation in the induced inelastic deformation to the bending loads. Transverse stiffeners are also needed for lateral stability requirements during bending since the spacing between point loads (L / 3 = 3.33 m) is larger than the limiting value (L_p = 1.1 m).

The accuracy of the point bending operation shows that the span length to radius of curvature ratio L / R = 10 / 7.5 = 1.33 is smaller than the limiting value of 1.5 and the ratio of the flange width to radius of curvature ratio b_f / R = 0.178 / 7.5 = 0.024 > 6.65 × (Δ_{res} / (L^2 / b_f)) = 6.65 × 34 × 10^{-4} = 0.023, that is satisfactory according to Eq. (7).

8.3 Solution for R = 5 m

If the radius of curvature R is reduced to 5 m, the span length to radius of curvature ratio L / R = 10 / 5 = 2 exceeds the limiting value of 1.5 specified in this paper. Consequently, point bending can be used only if the point loads are applied in two stages. In stage 1, the loads are applied to induce half the curvature (1 / R) e.g., twice the radius R (2 × 5 m = 10 m). In stage 2, they are applied to the already deformed shape from stage 1 to induce the remaining curvature.

The residual deformation Δ_{res} in each stage is calculated as a function of the radius R of 10 m induced in each stage $\Delta_{res} = 10\left(1-\sqrt{1-\left(\frac{10}{2\times 10}\right)^2}\right)$ = 1.34 m. From Fig. 7, based on $\Delta_{res} / (L^2 / b_f) \times 10{,}000 = 1.34 / (10^2 / 0.178) \times 10{,}000 = 23.9$, parameter χ is scaled as 0.669 (Grade 345). From Eq. (3), the point load P is calculated as $P = F_y t_f b_f^2 / \chi L$ = 345 × 1000 × 0.0128 × (0.1782^2) / 0.669 × 10 = 21 kN, almost equal to the 20.9 kN load used to induce the radius of 15 m and 21 kN load to induce the radius of 7.5 m. Note that transverse stiffeners are needed for lateral stability requirements during bending as in the previous cases.

The ratio of the flange width to radius of curvature ratio in each stage $b_f / R = 0.178 / 10 = 0.018 > 6.65 \times (\Delta_{res} / (L^2 / b_f)) = 6.65 \times 23.9 \times 10^{-4} = 0.016$, that is satisfactory according to Eq. (7).

8.4 Summary

The numerical application predicts that for a 10 m long W410 × 60 girder made of Grade 345, two point loads of 20.9 kN each spaced at 3.33 m (one third the span length) will induce a radius R of 15 m. These loads increase marginally to 21 kN to induce a radius R of 7.5 m (50% reduction). This insignificant difference in loads is due to the sensitivity of the variation in the induced deformations to the yield onset (Fig. 7). In both cases, the bending loads were smaller than the maximum flange buckling load of 424 kN and the radii of curvature were within the limits specified for applicability of the proposed point bending procedure ($L / R < 1.5$ and $b_f / R \geq 6.65 \times (\Delta_{res} / (L^2 / b_f))$.

For a radius of curvature of 5 m, the limit specified on the girder length to radius ratio ($L / R = 10 / 5 = 2 > 1.5$) was not satisfied which necessitated performing the point bending operation in two stages. In each stage a radius R of 10 m (2×5 m) was induced using a bending load of 21 kN. Note that the effects of residual stresses that build up from the bending in the first stage were not considered (Spoorenberg *et al*. 2010).

9. Conclusions

This paper examines the post-yield response of symmetric, wide-flange steel girders subjected to point load bending about its weak axis. A general theoretical framework relating loads and residual deformations to cross-sectional properties is developed for inducing horizontal circular curves. Point bending systems were consequently optimized from parametric and sensitivity analyses.

Based on the findings of this paper, it was shown that the most important variable that controls permanent residual deformations due to point loads is the location where yield initiates in the span shear span a'. This is given by distance x_2 (shown in Fig. 6) and depending on the cross-section, x_2 varies from $0.667a'$ to $0.695a'$. Within this range, a less than 1% reduction in x_2 can reduce the radius of curvature by more than half its value.

The theoretical solution focused on available AISC rolled wide flange sections (W1100 × 499 to W100 × 19.3) to set curvature and strain limits that could be attained without overstraining or damaging the steel section. It was shown that radii of curvatures R as little as 16.5 m (Grade 250), 12 m (Grade 345) and 10 m (Grade 415) for a flange width b_f = 457 mm and R = 4 m (Grade 250),

3 m (Grade 345) and 2.5 m (Grade 415) for b_f = 100mm can be induced with the maximum strain not exceeding 12.65 times the yield strain ε_y.

Overall, this paper shows that point bending is suitable for inducing parabolic deformed shapes that closely match circular curves if the girder length to radius of curvature ratio (L/R) is less than 1.5 and the bending loads are placed at the third points of the girder.

Finally, the analytical solutions presented in this paper are idealized and therefore their accuracy in predicting the deformation in the inelastic range cannot be exactly realized in practice even if actual (not nominal) material properties are used (Brocknebrough 2003). Nonetheless, the solutions facilitate understanding of the inelastic behavior of point load bending systems. This helps reduce trial and error in determining the capacity of hydraulic jacks and in evaluating alternative set-ups for the curving operation.

References

AISC (2011), Steel Construction Manual, (14th Edition), American Institute of Steel Construction, USA.

Alwood, T.A. (2006), "What engineers should know about bending steel", *Modern Steel Construction* (*MSC*), May, pp. 24-26.

Barnshaw, R. (2009), "Bending considerations in steel construction", *Modern Steel Construction* (*MSC*), October, pp. 42-44.

Bjorhovde, R. (2006), "Cold bending of wide-flange shapes for construction", *Am. Inst. Steel Construct.* (*AISC*), *Eng. J.*, **4**(43), 271-286.

Brockenbrough, R.L. (2003), "MTR survey of plate material used in structural fabrication", *Am. Inst. Steel Construct.* (*AISC*), *Eng. J.*, **40**(1), 42-49.

Craig, R.R. (2011), *Mechanics of Materials*, (3rd Edition), John Wiley and Sons, Inc.

Gergess, A. and Sen, R. (2010), "Post-yield response of cold-cambered wide-flange steel beams", *J. Construct. Steel Res.*, **65**(10), 1155-1163.

Gergess, A. and Sen, R. (2011), "Optimized solution for bending wide-flange steel beams about their weak axis", *Modern Method. Adv. Struct. Eng. Construct.*, Singapore, pp. 865- 870.

King, M. (2005), "Around the bend: What detailers should know about bending steel", *Modern Steel Construction* (*MSC*), May, pp. 61-63.

Lange, J. and Grages, H. (2009), "Influence of the Bauschinger effect on the deflection behaviour of cambered steel and steel concrete composite beams", *Struct. Eng. Int.*, **19**(4), 410-414.

Mansouri, H., Monshi, A. and Hadavinia, H. (2004), "Effect of local induction heat treatment on the induced residual stresses in the web region of a welded rail", *J. Strain Anal. Eng. Des.*, **39**(3), 271-283.

Moen, C. and Via, E.C. (2011), "Cold bending fabrication – state-of-the-art, industry challenges, engineering solutions, *TRB AFH70 Committee Meeting*, *Fabrication and Inspection of Metal Structures*, Washington, D.C., USA, January.

Salmon, C.G., Malhas F.A. and Johnson, J.E. (2010), *Steel Structures*: *Design and Behavior*, (5th Edition), Harper- Collins, NY, USA.

Spoorenberg, R.C., Snijder, H.H. and Hoenderkamp, J.C.D. (2010), "Experimental investigation of residual stresses in roller bent wide flange steel sections", *J. Construct. Steel Res.*, **66**(6), 737-747.

White, D.W. (2008), "Structural behavior of steel", *Steel Bridge Design Handbook*, Chapter 6, National Steel Bridge Alliance, Chicago, IL, USA.

Wong, E. and Driver, R.G. (2010), "Critical evaluation of equivalent moment factor procedures for laterally unsupported beams", *Eng. J. AISC*, **47**(1), 1-20.

DL